Table 4-1 Atomic mass excesses†

Z	*Element*	*A*	*M − A, Mev*
0	*n*	1	8.07144
1	H	1	7.28899
	D	2	13.13591
	T	3	14.94995
	H	4	28.22000
		5	31.09000
2	He	3	14.93134
		4	2.42475
		5	11.45400
		6	17.59820
		7	26.03000
		8	32.00000
3	Li	5	11.67900
		6	14.08840
		7	14.90730
		8	20.94620
		9	24.96500
4	Be	6	18.37560
		7	15.76890
		8	4.94420
		9	11.35050
		10	12.60700
		11	20.18100
5	B	7	27.99000
		8	22.92310
		9	12.41860
		10	12.05220
		11	8.66768
		12	13.37020
		13	16.56160
6	C	9	28.99000
		10	15.65800
		11	10.64840
		12	0
		13	3.12460
		14	3.01982
		15	9.87320
7	N	12	17.36400
		13	5.34520
		14	2.86373
		15	0.10040
		16	5.68510
		17	7.87100
8	O	14	8.00800
		15	2.85990
		16	−4.73655
		17	−0.80770
		18	−0.78243
		19	3.33270
		20	3.79900
9	F	16	10.90400
		17	1.95190
		18	0.87240
		19	−1.48600
		20	−0.01190
		21	−0.04600
10	Ne	18	5.31930
		19	1.75200
		20	−7.04150
		21	−5.72990
		22	−8.02490
		23	−5.14830
		24	−5.94900
11	Na	20	8.28000
		21	−2.18500
		22	−5.18220
		23	−9.52830
		24	−8.41840
		25	−9.35600
		26	−7.69000
12	Mg	22	−0.14000
		23	−5.47240
		24	−13.93330
		25	−13.19070
		26	−16.21420
		27	−14.58260
		28	−15.02000
13	Al	24	0.1000
		25	−8.9310
		26	−12.2108
		27	−17.1961
		28	−16.8554
		29	−18.2180
		30	−17.1500
14	Si	26	−7.1320
		27	−12.3860
		28	−21.4899
		29	−21.8936
		30	−24.4394
		31	−22.9620
		32	−24.2000
15	P	28	−7.6600
		29	−16.9450
		30	−20.1970
		31	−24.4376
		32	−24.3027

Table 4-1 Atomic masses excesses† (Continued)

Z	*Element*	*A*	*M − A, Mev*
15	P	33	−26.3346
		34	−24.8300
16	S	30	−14.0900
		31	−18.9920
		32	−26.0127
		33	−26.5826
		34	−29.9335
		35	−28.8471
		36	−30.6550
		37	−27.0000
		38	−26.8000
17	Cl	32	−12.8100
		33	−21.0140
		34	−24.4510
		35	−29.0145
		36	−29.5196
		37	−31.7648
		38	−29.8030
		39	−29.8000
		40	−27.5000
18	Ar	34	−18.3940
		35	−23.0510
		36	−30.2316
		37	−30.9509
		38	−34.7182
		39	−33.2380
		40	−35.0383
		41	−33.0674
		42	−34.4200
19	K	36	−16.7300
		37	−24.8100
		38	−28.7860
		39	−33.8033
		40	−33.5333
		41	−35.5524
		42	−35.0180
		43	−36.5790
		44	−35.3600
		45	−36.6300
		46	−35.3400
		47	−36.2500
20	Ca	38	−21.6900
		39	−27.3000
		40	−34.8476
		41	−35.1400
		42	−38.5397
		43	−38.3959
		44	−41.4596
		45	−40.8085
		46	−43.1380
		47	−42.3470
		48	−44.2160
		49	−41.2880
21	Sc	40	−20.9000
		41	−28.6450
		42	−32.1410
		43	−36.1740
		44	−37.8130
		45	−41.0606
		46	−41.7557
		47	−44.3263
		48	−44.5050
		49	−46.5490
		50	−44.9600
22	Ti	42	−25.1230
		43	−29.3400
		44	−37.6580
		45	−39.0020
		46	−44.1226
		47	−44.9266
		48	−48.4831
		49	−48.5577
		50	−51.4307
		51	−49.7380
		52	−49.5400
23	V	46	−37.0600
		47	−42.0100
		48	−44.4700
		49	−47.9502
		50	−49.2158
		51	−52.1989
		52	−51.4360
		53	−52.1800
		54	−49.6300
24	Cr	48	−42.8130
		49	−45.3900
		50	−50.2490
		51	−51.4472
		52	−55.4107
		53	−55.2807
		54	−56.9305
		55	−55.1130
		56	−55.2900
25	Mn	50	−42.6480
		51	−48.2600
		52	−50.7020

Table 4-1 Atomic mass excesses† (Continued)

Z	*Element*	*A*	*M − A, Mev*
25	Mn	53	−54.6820
		54	−55.5520
		55	−57.7048
		56	−56.9038
		57	−57.4800
		58	−55.6500
26	Fe	52	−48.3280
		53	−50.6930
		54	−56.2455
		55	−57.4735
		56	−60.6054
		57	−60.1755
		58	−62.1465
		59	−60.6599
		60	−61.5110
		61	−59.1300
27	Co	54	−47.9940
		55	−54.0140
		56	−56.0310
		57	−59.3389
		58	−59.8380
		59	−62.2327
		60	−61.6513
		61	−62.9300
		62	−61.5280
		63	−61.9200
28	Ni	56	−53.8990
		57	−56.1040
		58	−60.2280
		59	−61.1587
		60	−64.4707
		61	−64.2200
		62	−66.7480
		63	−65.5160
		64	−67.1060
		65	−65.1370
		66	−66 0550
29	Cu	58	−51.6590
		59	−56.3590
		60	−58.3460
		61	−61.9840
		62	−62.8130
		63	−65.5831
		64	−65.4276
		65	−67.2660
		66	−66.2550
		67	−67.2910
		68	−65.4100
30	Zn	60	−54.1860
		61	−56.5800
		62	−61.1230
		63	−62.2170
		64	−66.0003
		65	−65.9170
		66	−68.8810
		67	−67.8630
		68	−69.9940
		69	−68.4250
		70	−69.5500
		71	−67.5200
		72	−68.1440
31	Ga	63	−56.7200
		64	−58.9280
		65	−62.6580
		66	−63.7060
		67	−66.8650
		68	−67.0740
		69	−69.3262
		70	−68.8970

† Based on the scale $C^{12} = 0$; 1 amu = 931.478 Mev. This table of masses, prepared by T. Lauritsen, is largely adapted from the comprehensive review by J. H. E. Mattauch, W. Thiele, and A. H. Wapstra, *Nucl. Phys.*, 67:1 (1965). Terminal zeros are generally not significant digits.

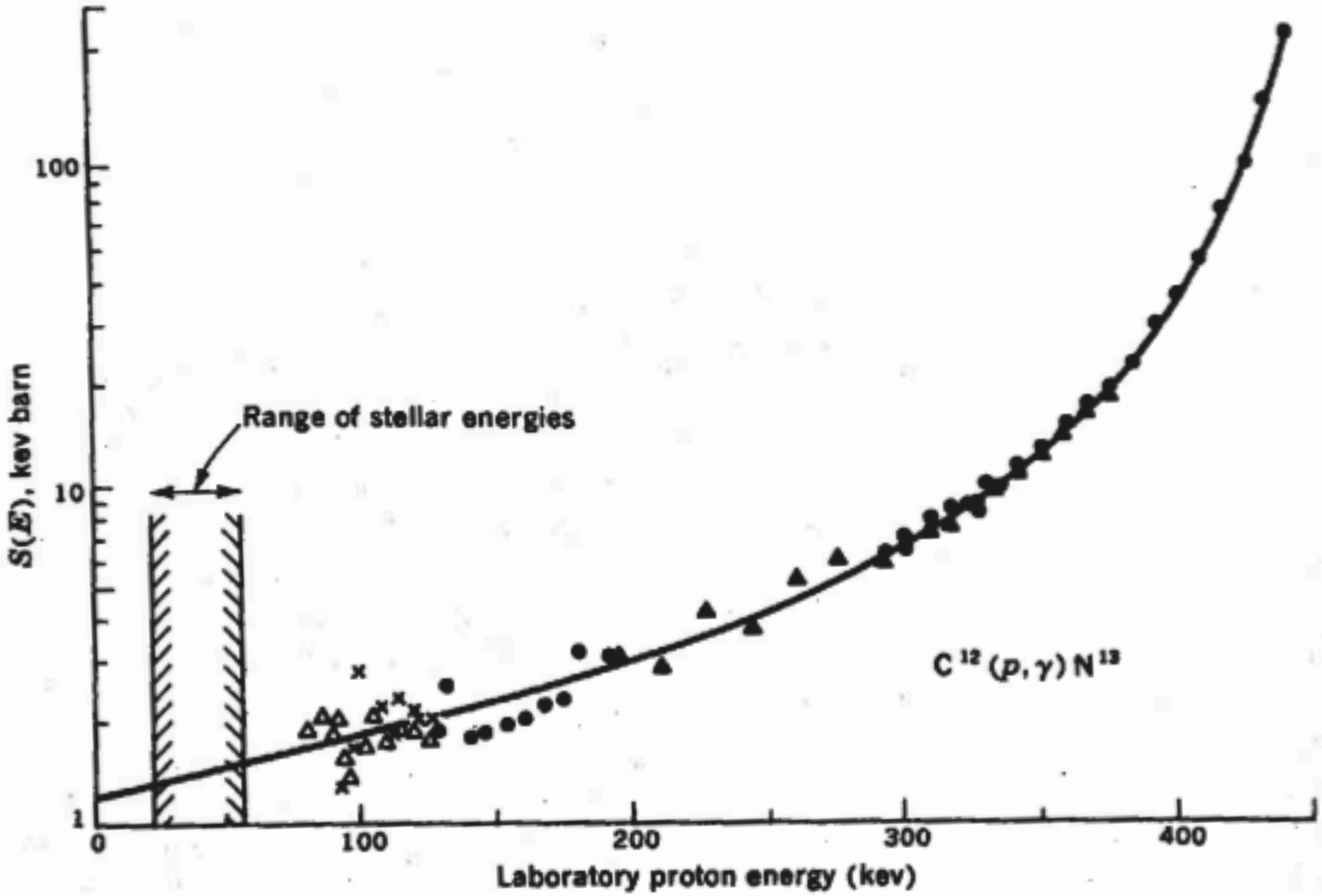

Fig. 4-5 The cross-section factor $S(E)$ for the radiative capture of protons by C^{12}. The differing types of data points represent five different experiments performed at different times and laboratories by the workers indicated. Detailed references and discussion may be found in D. F. Hebbard and J. L. Vogl, *Nucl. Phys.*, **21**:652 (1960). This curve is more readily extrapolated than the one in Fig. 4-4.

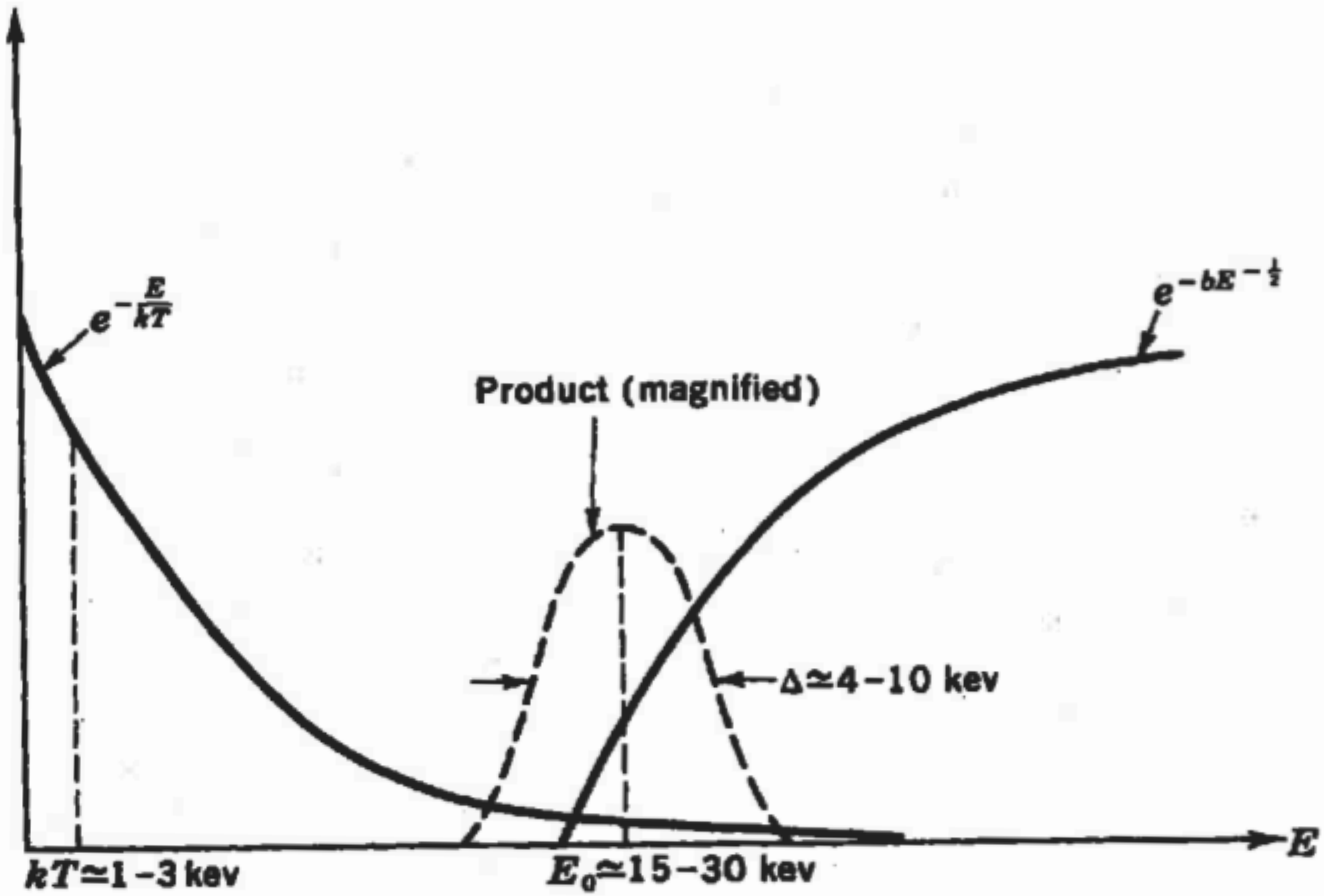

Fig. 4-6 The dominant energy-dependent factors in thermonuclear reactions. Most of the reactions occur in the high-energy tail of the maxwellian energy distribution, which introduces the rapidly falling factor $\exp(-E/kT)$. Penetration through the coulomb barrier introduces the factor $\exp(-bE^{-\frac{1}{2}})$, which vanishes strongly at low energy. Their product is a fairly sharp peak near an energy designated by E_0, which is generally much larger than kT. The peak is pushed out to this energy by the penetration factor, and it is therefore commonly called the *Gamow peak* in honor of the physicist who first studied the penetration through the coulomb barrier.

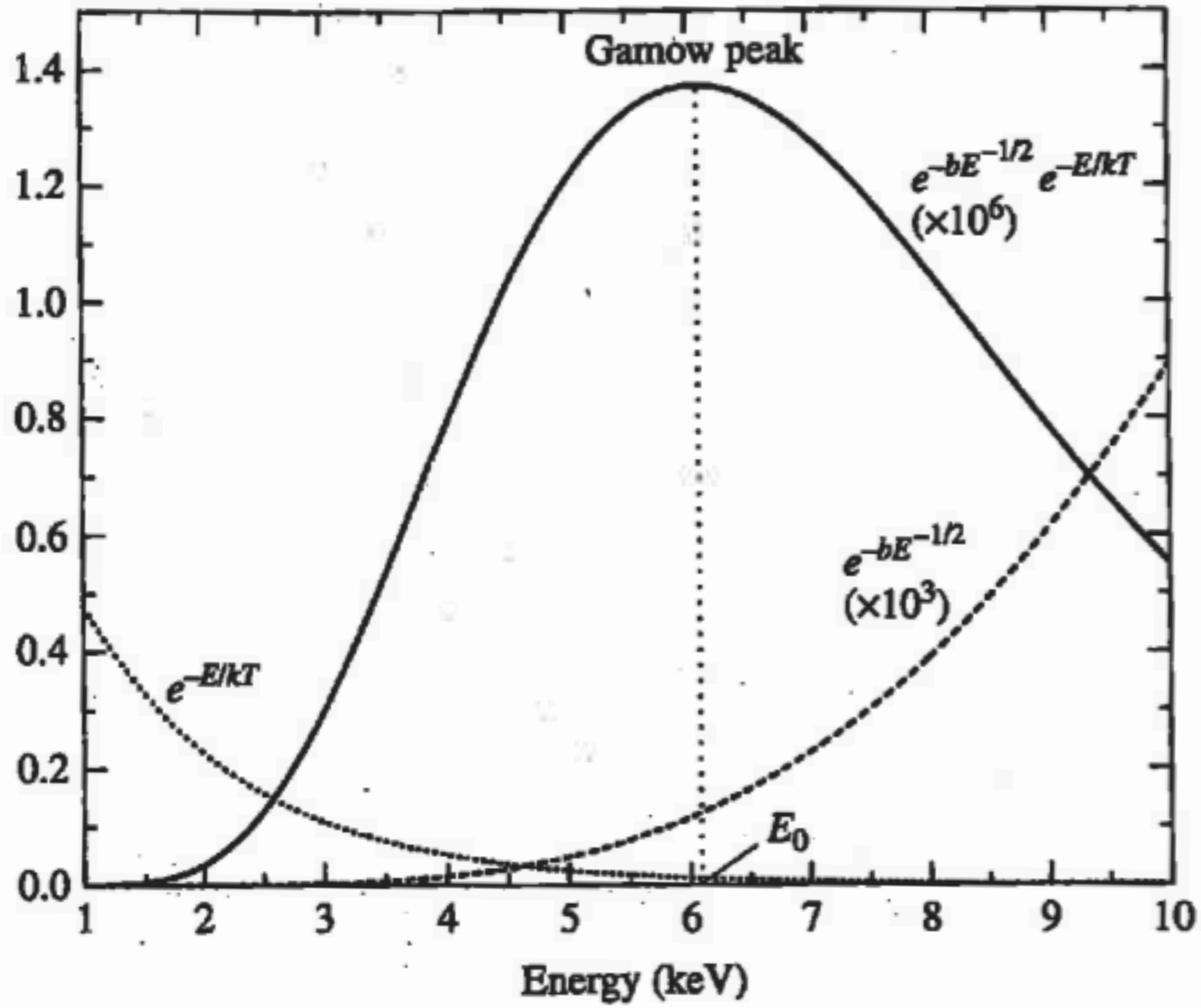

FIGURE 10.6 The likelihood that a nuclear reaction will occur is a function of the kinetic energy of the collision. The Gamow peak arises from the contribution of the $e^{-E/kT}$ Maxwell–Boltzmann high-energy tail and the $e^{-bE^{-1/2}}$ Coulomb barrier penetration term. This particular example represents the collision of two protons at the central temperature of the Sun. (Note that $e^{-bE^{-1/2}}$ and $e^{-bE^{-1/2}}e^{-E/kT}$ have been multiplied by 10^3 and 10^6, respectively, to more readily illustrate the functional dependence on energy.)

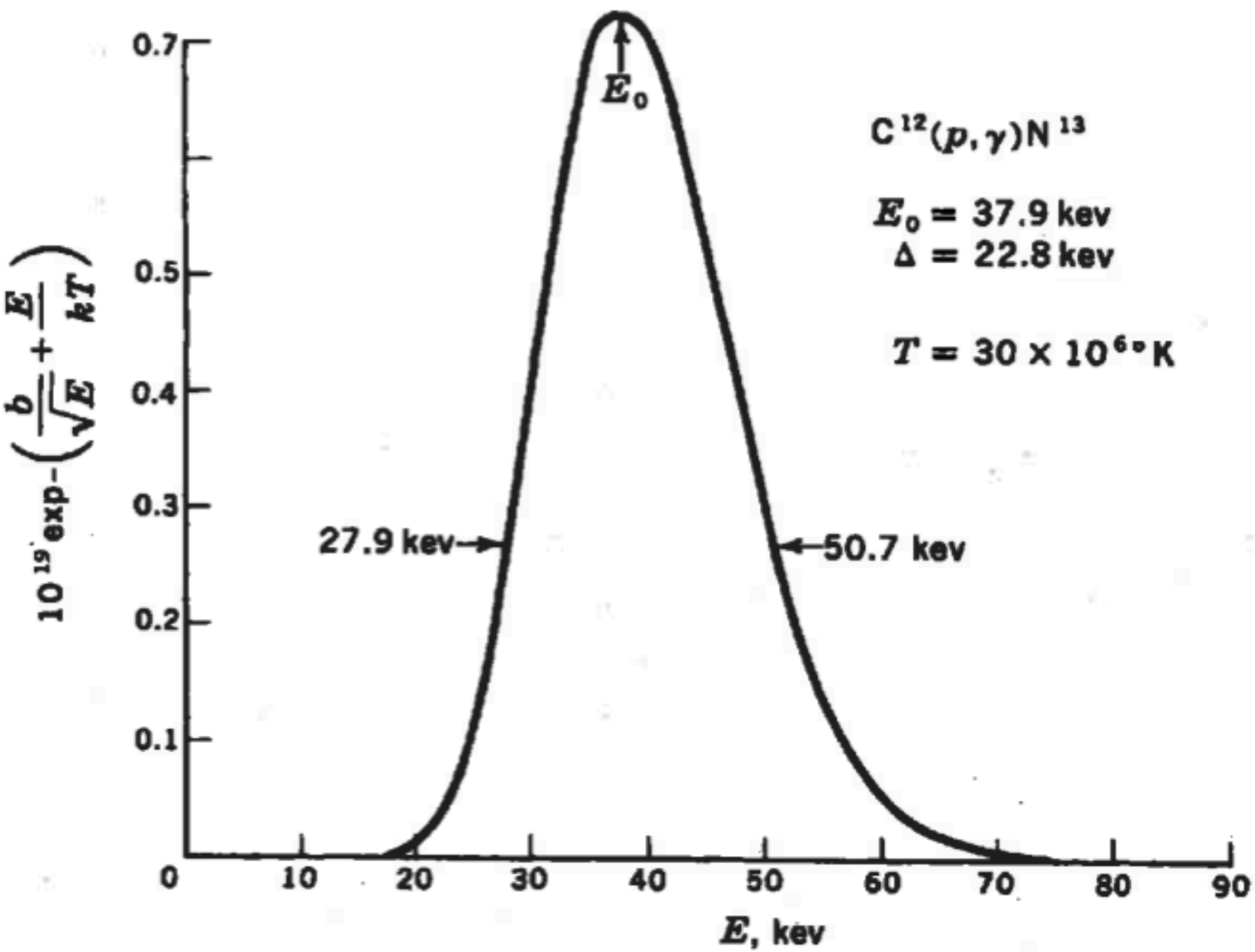

Fig. 4-7 The Gamow peak for the reaction $C^{12}(p,\gamma)N^{13}$ at $T = 30 \times 10^6$ °K. The curve is actually somewhat asymmetric about E_0, but it is nonetheless adequately approximated by a gaussian.

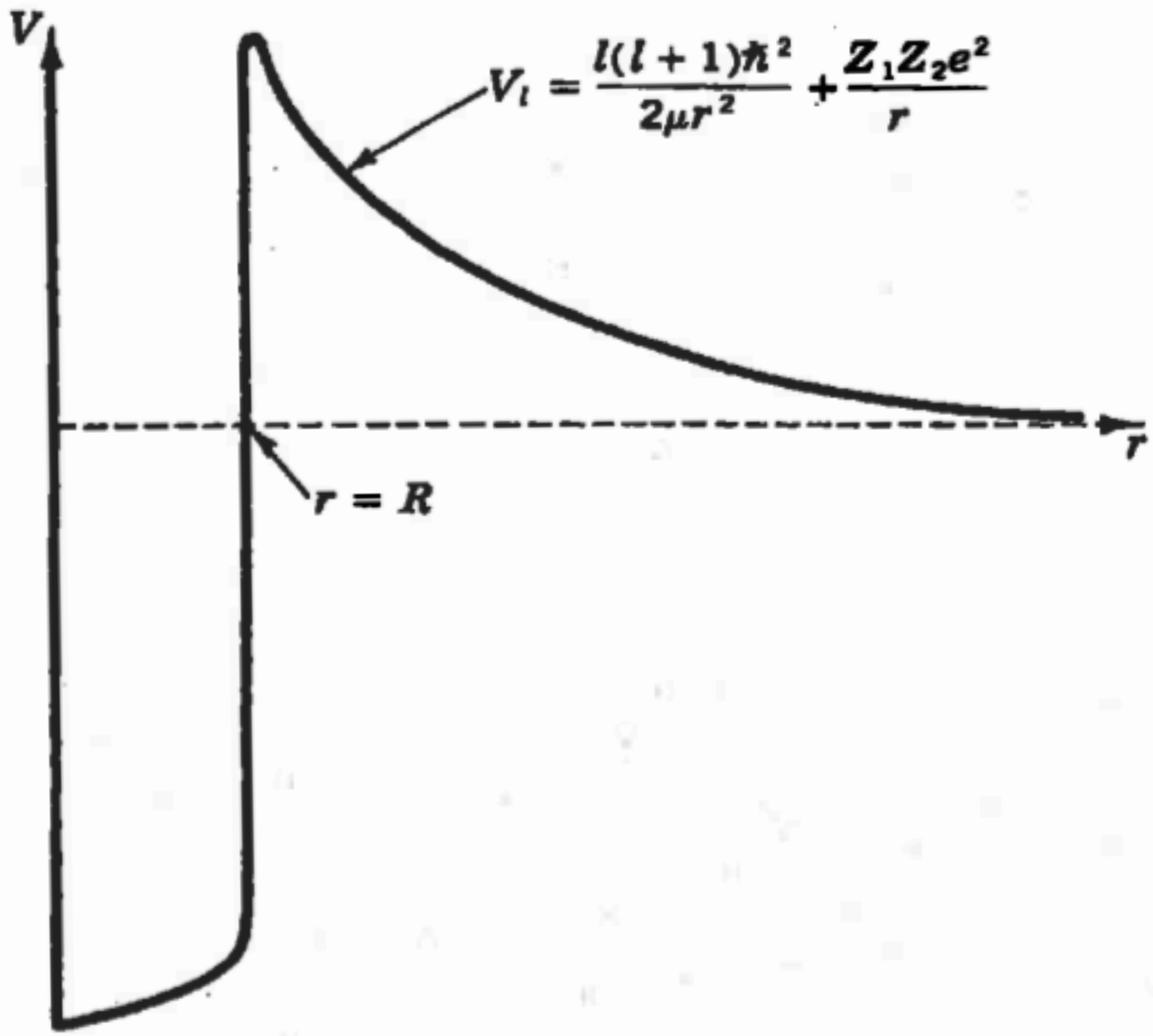

Fig. 4-11 The potential governing the motion of one nucleus relative to another. For $r < R$ the nuclei are essentially in contact, and the strongly attractive short-range nuclear force results in a deep negative potential. For $r > R$ the nuclear force can no longer be felt, and the coulomb potential dominates. When one considers the radial motion of the two nuclei, the angular momentum adds an effective centrifugal potential. The total extranuclear radial potential is designated by V_l.

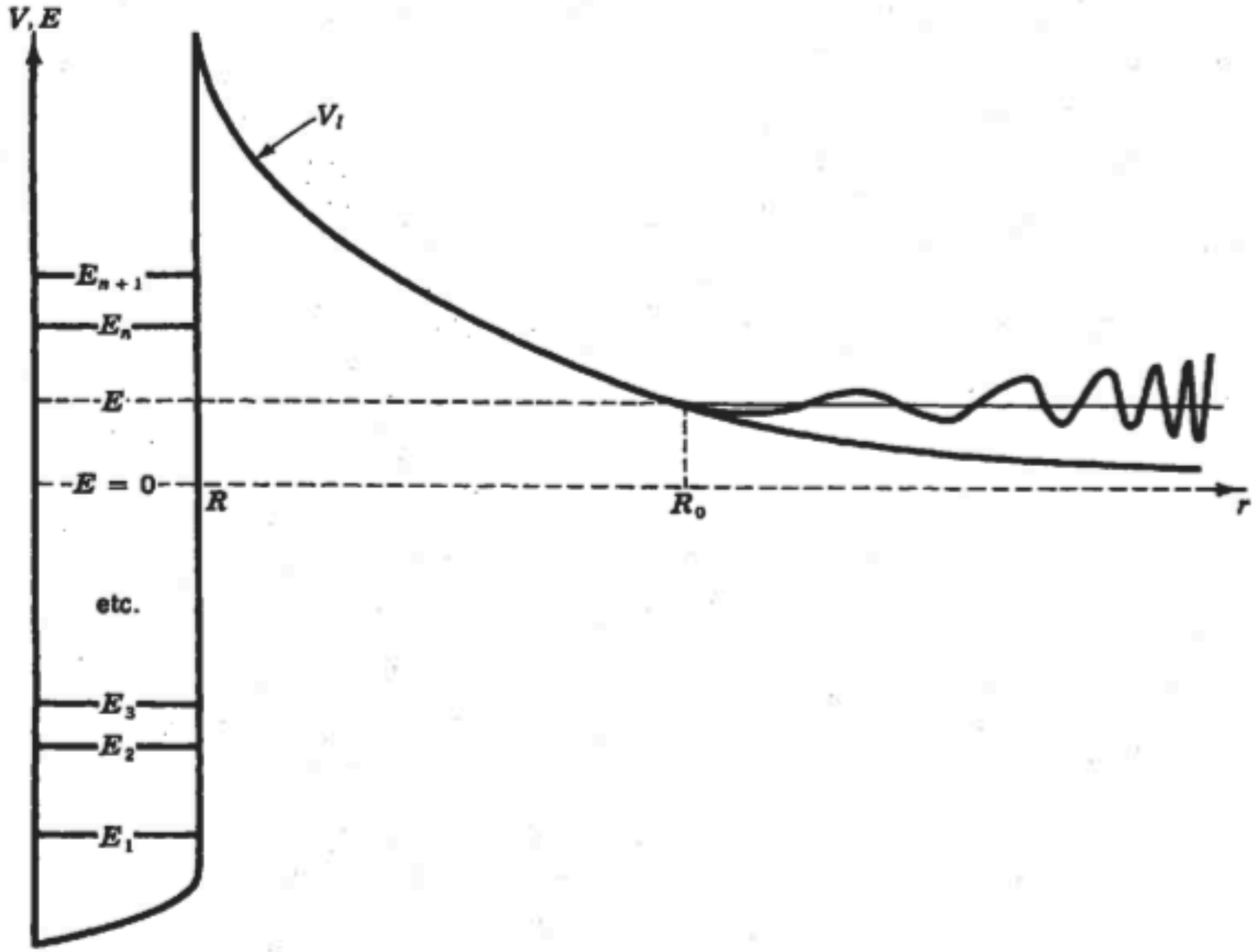

Fig. 4-12 The stationary nuclear states in the compound nucleus formed by the coalescence of the two colliding particles are designated by E_1, E_2, ... The increasing wavelength of the incoming wave reflects the loss of momentum as the kinetic energy E is expended against the repulsive extranuclear potential V_l. Within the context of classical mechanics the incoming particle would be expected to rebound from the potential at the classical turning point R_0, but in the quantum treatment the wave has a nonzero probability of tunneling through the potential barrier to the interaction radius R. The compound nucleus formed has an energy E that, in this case, falls between the natural resonances of the compound nucleus, so that the cross section will have a slowly varying dependence on the energy. The zero of energy is determined relative to the ground state E_1 of the compound nucleus by the extra mass of the colliding particles.

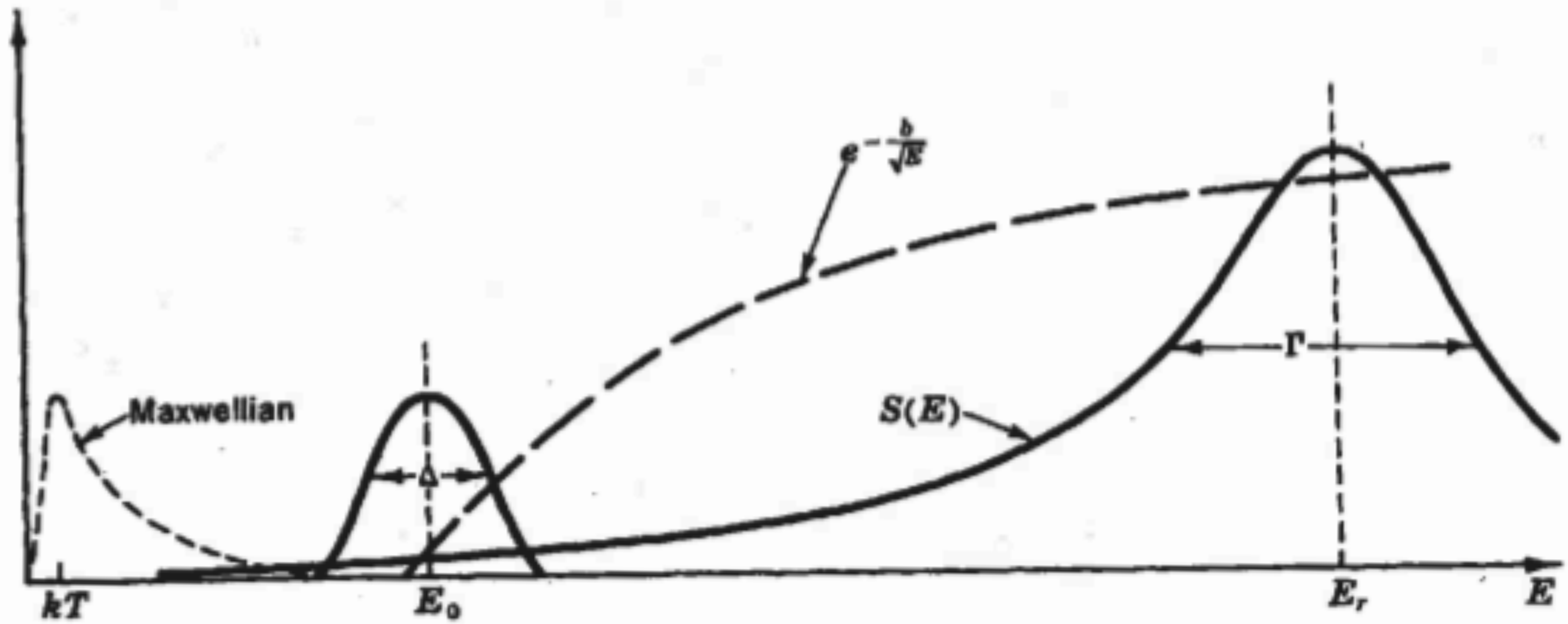

Fig. 4-22 A schematic representation of the major energy-dependent factors for a reaction, like that in Fig. 4-21, which proceeds through the wing of a broad distant resonance. In such a case the nonresonant-reaction formulation is used, and $S(E)$ is calculable by Eq. (4-188).

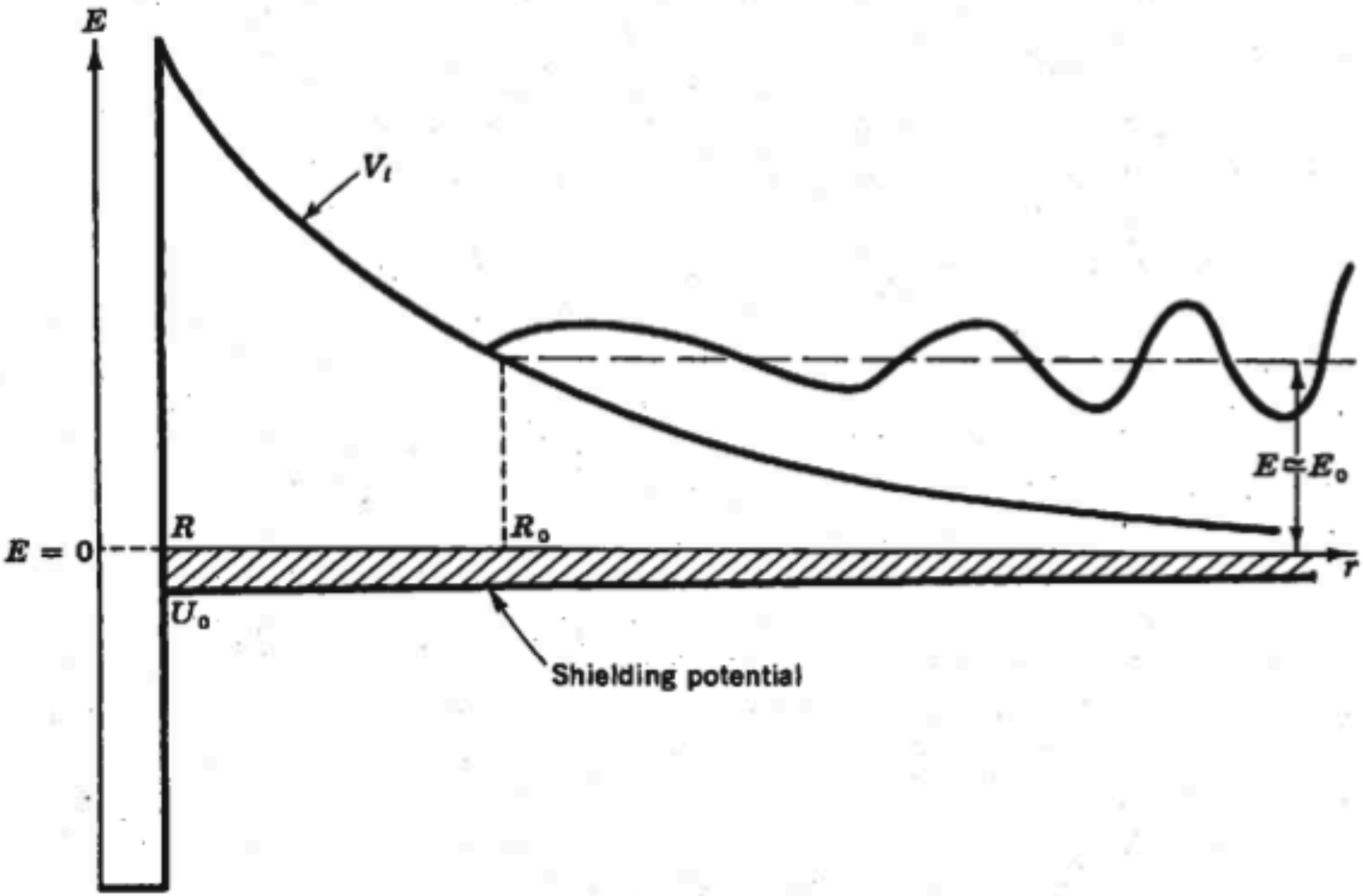

Fig. 4-24 The effective radial potential V_l modified by the screening potential. The polarization of the electron-ion plasma results in a small attractive potential, which is here drawn beneath the $E = 0$ axis. This small negative potential has the effect of reducing V_l and thereby increasing the penetrability of the barrier.

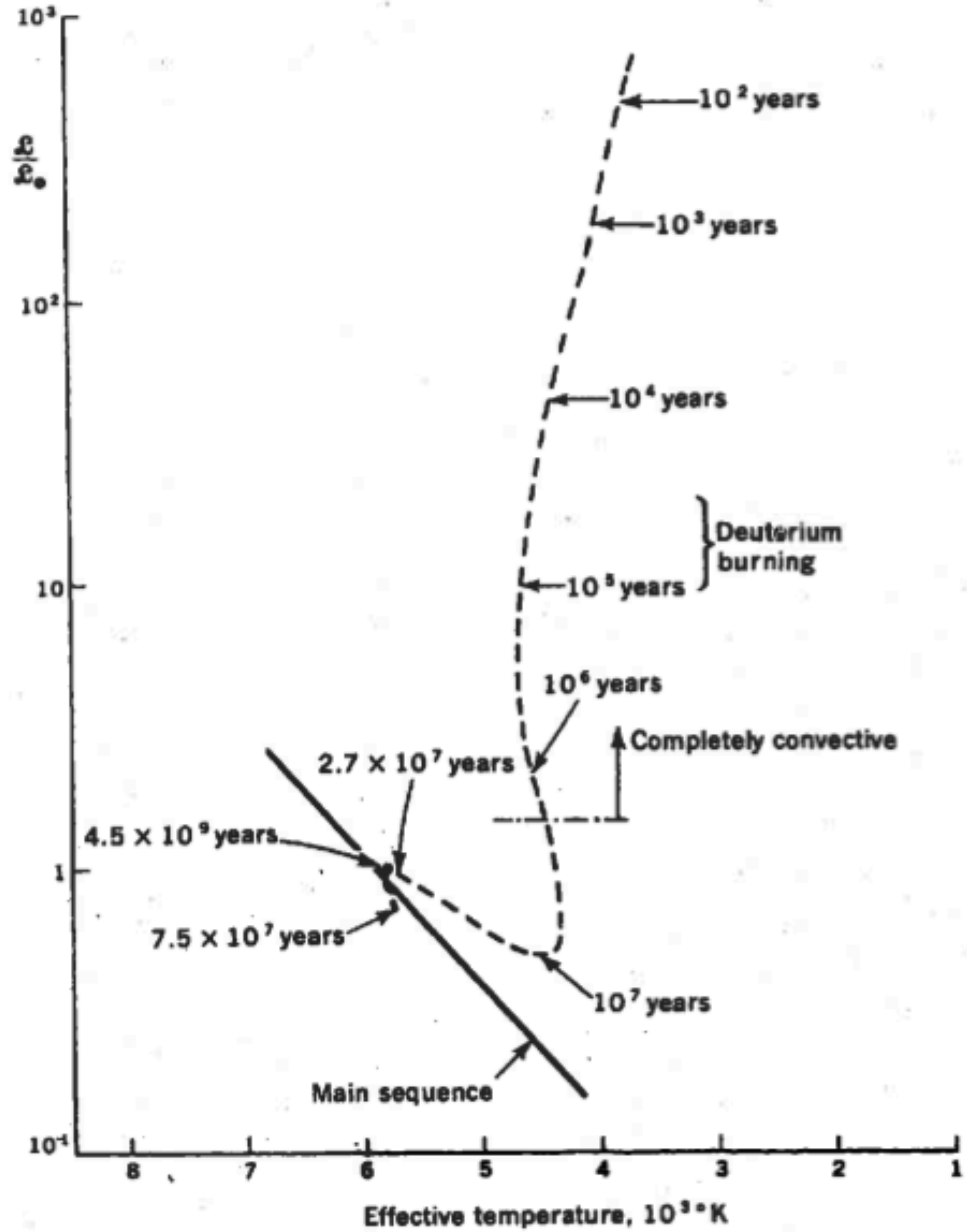

Fig. 5-1 The path on the H-R diagram of the contraction of the sun to the main sequence. The interior has become sufficiently hot to burn deuterium after about 10^5 years. The contraction ceases near the main sequence when the core has become hot enough to replenish the solar luminosity with the thermonuclear power generated by the fusion of hydrogen into helium. [*After D. Ezer and A. G. W. Cameron, The Contraction Phase of Stellar Evolution, in R. F. Stein and A. G. W. Cameron (eds.), "Stellar Evolution," Plenum Press, New York,* 1966.]

Table 5-1 Reactions of the PP chains

Reaction	*Q* value, Mev	Average ν loss, Mev	S_0, kev barns	$\frac{dS}{dE}$, barns	*B*	τ_{12}, years†
$H^1(p,\beta^+\nu)D^2$	1.442	0.263	3.78×10^{-22}	4.2×10^{-24}	33.81	7.9×10^{9}
$D^2(p,\gamma)He^3$	5.493		2.5×10^{-4}	7.9×10^{-6}	37.21	4.4×10^{-8}
$He^3(He^3,2p)He^4$	12.859		5.0×10^{3}		122.77	2.4×10^{5}
$He^3(\alpha,\gamma)Be^7$	1.586		4.7×10^{-1}	-2.8×10^{-4}	122.28	9.7×10^{5}
$Be^7(e^-,\nu)Li^7$	0.861	0.80				3.9×10^{-1}
$Li^7(p,\alpha)He^4$	17.347		1.2×10^{2}		84.73	1.8×10^{-5}
$Be^7(p,\gamma)B^8$	0.135		4.0×10^{-2}		102.65	6.6×10^{1}
$B^8(\beta^+\nu)Be^{8*}(\alpha)He^4$	18.074	7.2				3×10^{-8}

† Computed for $X = Y = 0.5$, $\rho = 100$, $T_6 = 15$ (sun).

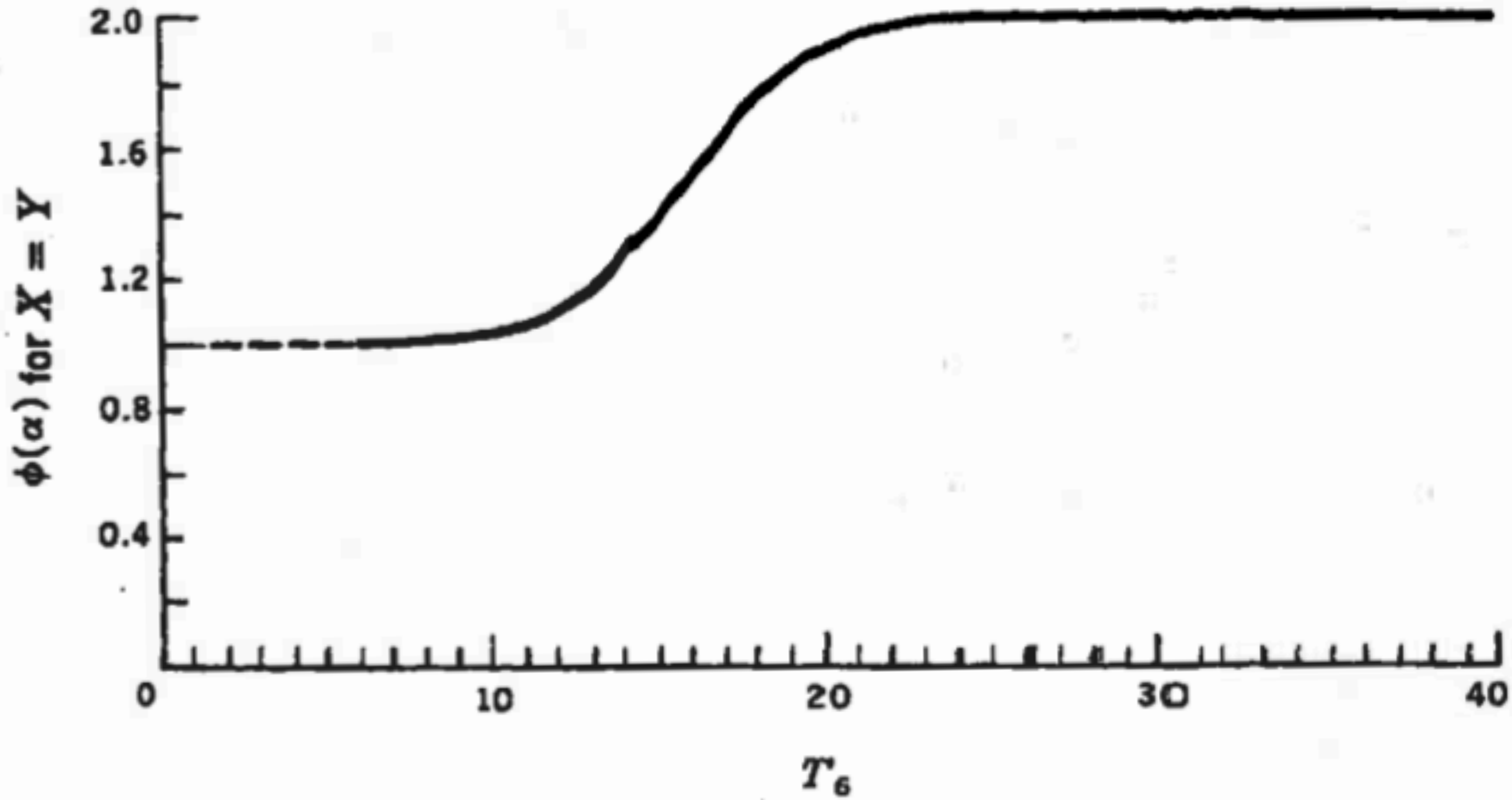

Fig. 5-9 The rate of production of He^4 is increased over its rate in PPI by a factor $\Phi(\alpha)$, which is shown here as a function of temperature for the particular composition $X = Y$. [*After P. D. Parker, J. N. Bahcall, and W. A. Fowler, Astrophys. J.*, **139**:602 (1964). *By permission of The University of Chicago Press. Copyright* 1964 *by The University of Chicago.*]

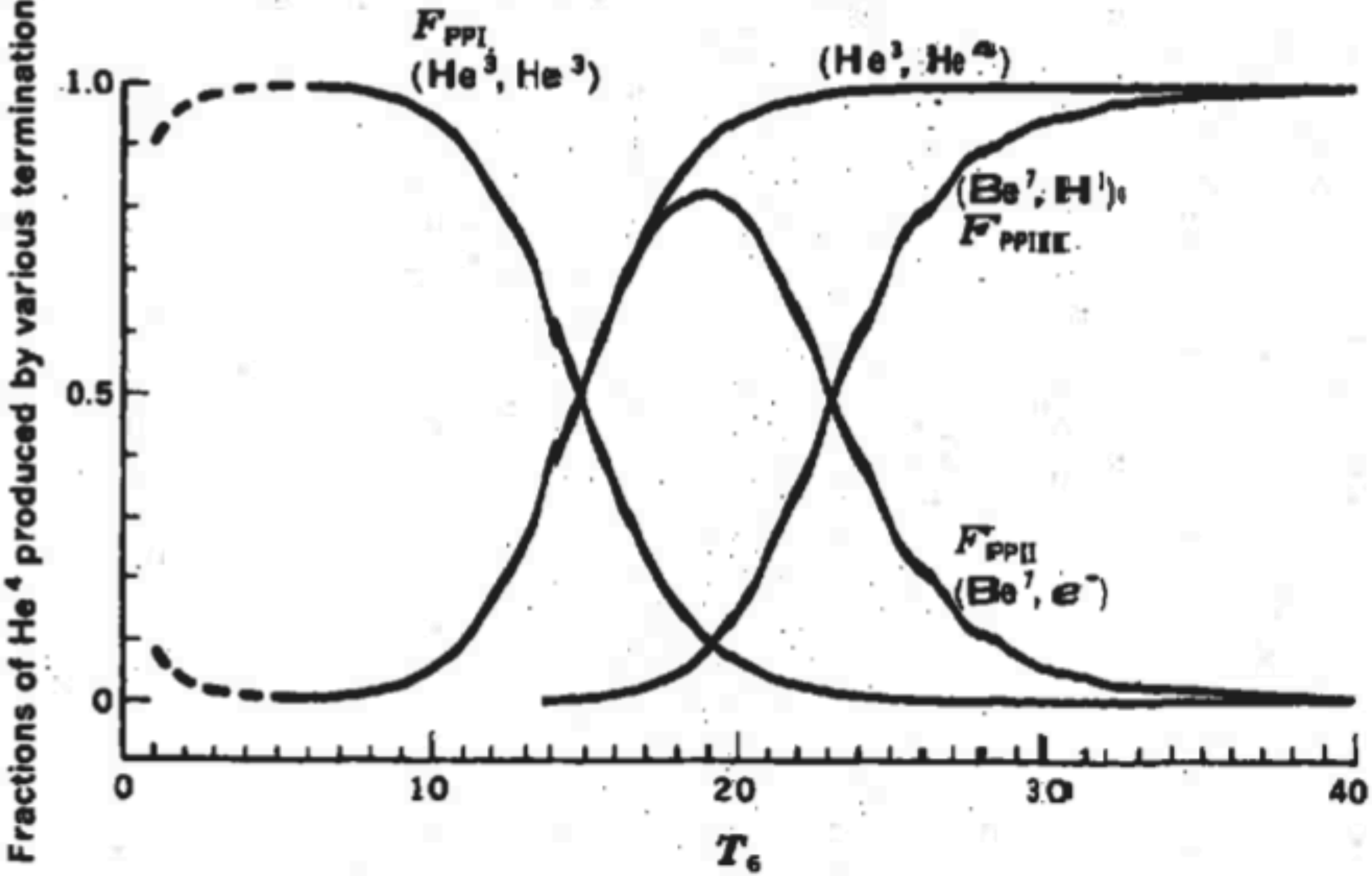

Fig. 5-10 The fraction of the He^4 production due to PPI, PPII, and PPIII, respectively. The chains are assumed to be in equilibrium, and for the purpose of this figure it was assumed that $Y = X$. [*After P. D. Parker, J. N. Bahcall, and W. A. Fowler, Astrophys. J.,* 139:602 (1964). *By permission of The University of Chicago Press. Copyright* 1964 *by The University of Chicago.*]

Table 5-2 The CNO reactions

Reaction	*Q value, Mev*	*Average ν loss, Mev*	*$S(E = 0)$, kev barns*	*$\frac{dS}{dE}$, barns*	*B*
$C^{12}(p,\gamma)N^{13}$	1.944		1.40	4.26×10^{-3}	136.93
$N^{13}(\beta^+\nu)C^{13}$	2.221	0.710			
$C^{13}(p,\gamma)N^{14}$	7.550		5.50	1.34×10^{-2}	137.20
$N^{14}(p,\gamma)O^{15}$	7.293		2.75		152.31
$O^{15}(\beta^+,\nu)N^{15}$	2.761	1.00			
$N^{15}(p,\alpha)C^{12}$	4.965		5.34×10^4	8.22×10^2	152.54
$N^{15}(p,\gamma)O^{16}$	12.126		2.74×10^1	1.86×10^{-1}	152.54
$O^{16}(p,\gamma)F^{17}$	0.601		1.03×10^1	-2.81×10^{-2}	166.96
$F^{17}(\beta^+\nu)O^{17}$	2.762	0.94			
$O^{17}(p,\alpha)N^{14}$	1.193		Resonant reaction		167.15

Table 5-3 Dependence of $\log (\tau_p \rho X_H/100)$ on temperature†

Temperature, T_6	*Reaction‡*						
	$C^{12}(p,\gamma)N^{13}$	$C^{13}(p,\gamma)N^{14}$	$N^{14}(p,\gamma)O^{15}$	$N^{15}(p,\alpha)C^{12}$	$10^4\gamma$	$O^{16}(p,\gamma)F^{17}$	$O^{17}(p,\alpha)N^{14}$
5	16.32	15.73	19.79	15.53	4.649	22.95	21.92
6	14.32	13.73	17.57	13.29	4.598	20.51	20.02
7	12.72	12.13	15.79	11.50	4.551	18.56	18.26
8	11.41	10.81	14.32	10.03	4.508	16.95	16.50
9	10.29	9.69	13.08	8.78	4.468	15.59	15.10
10	9.33	8.73	12.02	7.70	4.431	14.42	14.05
11	8.50	7.90	11.09	6.76	4.396	13.39	13.15
12	7.75	7.15	10.26	5.93	4.363	12.49	12.38
13	7.09	6.49	9.52	5.18	4.332	11.68	11.68
14	6.49	5.89	8.86	4.51	4.303	10.95	11.02
15	5.95	5.35	8.26	3.90	4.275	10.29	10.32
16	5.45	4.85	7.71	3.34	4.248	9.68	9.55
17	5.00	4.39	7.20	2.83	4.223	9.13	8.70
18	4.58	3.97	6.73	2.35	4.198	8.61	7.86
19	4.18	3.58	6.30	1.91	4.175	8.14	7.01
20	3.82	3.21	5.89	1.50	4.152	7.69	6.18
22	3.16	2.55	5.16	0.75	4.110	6.89	4.78
24	2.57	1.97	4.51	0.09	4.071	6.18	3.63
25	2.30	1.70	4.21	−0.21	4.052	5.85	3.10
26	2.05	1.44	3.93	−0.50	4.034	5.54	2.62
28	1.58	0.97	3.41	−1.03	4.000	4.97	1.75
30	1.15	0.54	2.93	−1.51	3.967	4.45	1.05
35	0.23	−0.38	1.91	−2.55	3.893	3.33	−0.42
40	−0.53	−1.14	1.07	−3.42	3.829	2.41	−1.50
45	−1.18	−1.78	0.36	−4.14	3.771	1.64	−2.33
50	−1.73	−2.33	−0.25	−4.77	3.719	0.97	−2.99
55	−2.21	−2.82	−0.78	−5.32	3.673	0.39	−3.53
60	−2.64	−3.24	−1.25	−5.81	3.630	−0.12	−3.97
65	−3.02	−3.63	−1.67	−6.24	3.590	−0.58	−4.33
70	−3.37	−3.97	−2.05	−6.63	3.554	−0.99	−4.65
75	−3.68	−4.28	−2.39	−6.99	3.521	−1.37	−4.91
80	−3.97	−4.57	−2.71	−7.32	3.489	−1.71	−5.14
85	−4.23	−4.83	−2.99	−7.62	3.460	−2.02	−5.35
90	−4.48	−5.08	−3.26	−7.90	3.433	−2.31	−5.52
95	−4.70	−5.30	−3.51	−8.15	3.407	−2.58	−5.68
100	−4.91	−5.51	−3.74	−8.39	3.383	−2.83	−5.82

† Adapted from G. R. Caughlan and W. A. Fowler, *Astrophys. J.*, **136**:453 (1962). By permission of The University of Chicago Press. Copyright 1962 by The University of Chicago.

‡ The lifetimes against protons are expressed in years, and the density ρ is in grams per cubic centimeter.

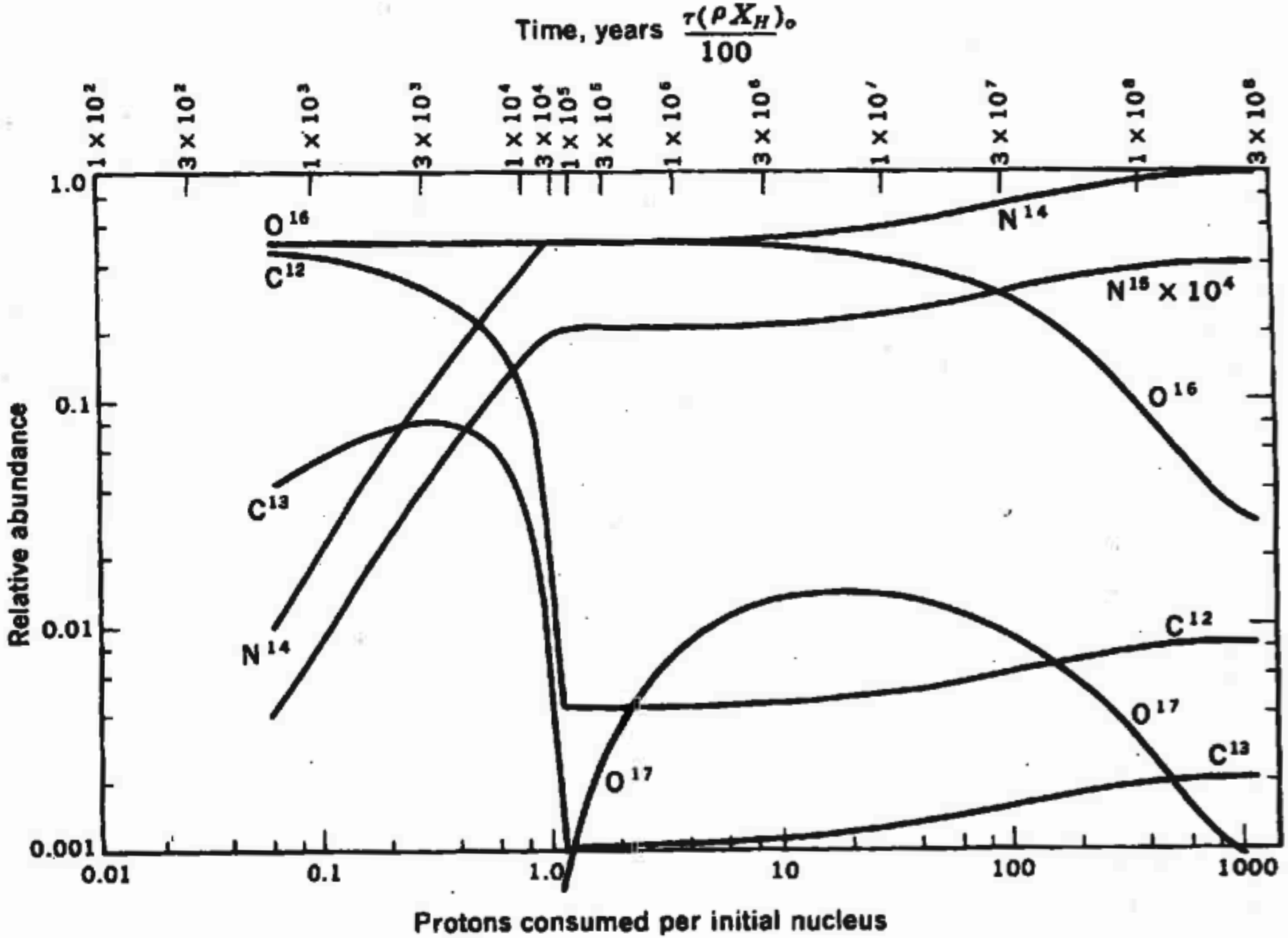

Fig. 5-15 The approach to equilibrium in the CNO bi-cycle as a function of the number of protons captured per initial CNO nucleus. This particular calculation started with equal concentrations of C^{12} and O^{16}. [*After G. R. Caughlan, Astrophys. J.*, **141**:688 (1965). *By permission of The University of Chicago Press. Copyright* 1964 *by The University of Chicago.*]

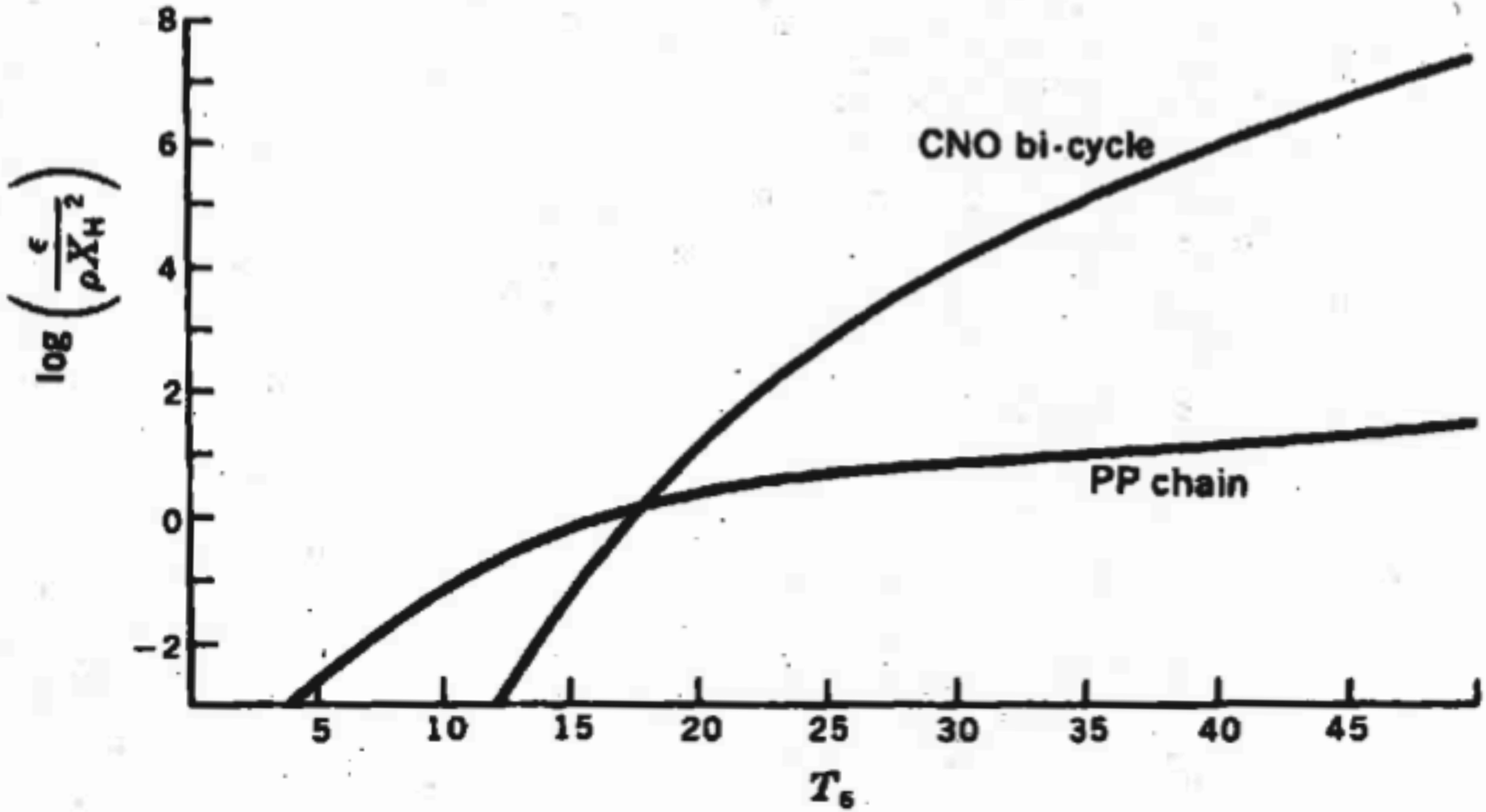

Fig. 5-16 A comparison of thermonuclear power from the P.P chains and the CNO cycle. Both chains are assumed to be operating in equilibrium. The calculation was made for the choice $X_{CN}/X_H = 0.02$, which is representative of population I composition.

Table 5-4 Helium-burning lifetimes

T_8	$\tau_{3\alpha}(\mathrm{He}^4)\left(\frac{\rho X_\alpha}{10^5}\right)^2$, years	$\tau_\alpha(\mathrm{C}^{12})\,\frac{\rho X_\alpha}{10^5}$, years	$\tau_\alpha(\mathrm{O}^{16})\,\frac{\rho X_\alpha}{10^5}$, years
0.8	1.0×10^{12}		
0.9	3.9×10^{9}	9.3×10^{8}	
1.0	4.2×10^{7}	9.6×10^{7}	1.1×10^{15}
1.1	1.1×10^{6}	1.3×10^{7}	7.7×10^{13}
1.2	5.2×10^{4}	2.3×10^{6}	7.7×10^{12}
1.3	4.1×10^{3}	4.9×10^{5}	9.6×10^{11}
1.4	4.6×10^{2}	1.2×10^{5}	1.5×10^{11}
1.5	7.2×10	3.3×10^{4}	2.6×10^{10}
1.6	1.4×10	1.0×10^{4}	5.8×10^{9}
1.7	3.4	3.6×10^{3}	1.4×10^{9}
1.8	1.0	1.4×10^{3}	3.8×10^{8}
1.9	3.3×10^{-1}	5.4×10^{2}	1.1×10^{8}
2.0	1.2×10^{-1}	2.4×10^{2}	3.6×10^{7}
2.1	4.9×10^{-2}	1.0×10^{2}	1.0×10^{7}
2.2	2.3×10^{-2}	5.1×10	1.2×10^{6}
2.3	1.1×10^{-2}	2.6×10	1.5×10^{5}
2.4	5.5×10^{-3}	1.3×10	2.4×10^{4}
2.5	3.2×10^{-3}	7.2	4.4×10^{3}
2.6	1.8×10^{-3}	4.0	9.3×10^{2}
2.8	6.6×10^{-4}	1.4	5.6×10
3.0	2.9×10^{-4}	5.2×10^{-1}	5.0
3.2	1.4×10^{-4}	2.1×10^{-1}	6.2×10^{-1}
3.4	7.5×10^{-5}	9.6×10^{-2}	9.6×10^{-2}
3.6	4.5×10^{-5}	4.5×10^{-2}	1.9×10^{-2}
3.8	2.9×10^{-5}	2.3×10^{-2}	4.3×10^{-3}
4.0	1.9×10^{-5}	1.2×10^{-2}	1.2×10^{-3}

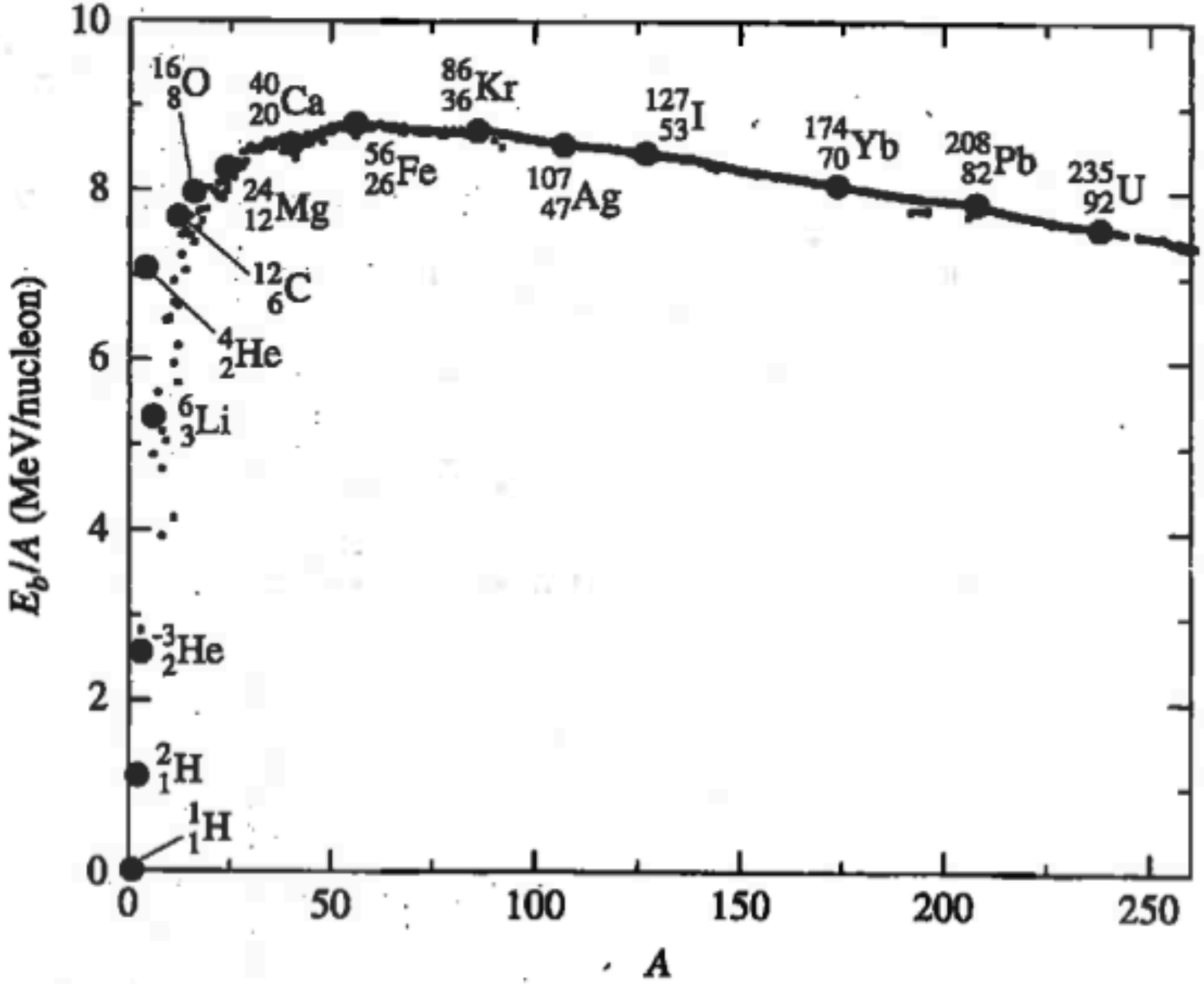

FIGURE 10.9 The binding energy per nucleon, E_b/A, as a function of mass number, A. Notice that several nuclei, most notably $^{4}_{2}$He (see also $^{12}_{6}$C and $^{16}_{8}$O), lie well above the general trend of the other nuclei, indicating unusual stability. At the peak of the curve is $^{56}_{26}$Fe, the most stable of all nuclei.